The Astrophysical Journal Letters, 864:L31 (7pp), 2018 September 10 https://doi.org/10.3847/2041-8213/aadc09

Widespread CCH and c-C_3H_2 in the Helix Nebula: Unraveling the Chemical History of Hydrocarbons

D. R. Schmidt[1], L. N. Zack[2], and L. M. Ziurys[1,3]
[1] Department of Astronomy and Steward Observatory, University of Arizona, 933 North Cherry Avenue, Tucson, AZ 85721-0065, USA
[2] Austin College, 900 North Grand Avenue, Sherman, TX 75090, USA
[3] Department of Chemistry and Biochemistry, University of Arizona, 1305 East 4th Street, Tucson, AZ 85719, USA
Received 2018 May 8; revised 2018 August 11; accepted 2018 August 20; published 2018 September 7

Abstract

The hydrocarbons CCH and c-C_3H_2 have been detected at multiple positions distributed across the Helix, along with the CN, indicating that these molecules are present throughout this very old planetary nebula. The species were identified by observations of the $N = 1 \rightarrow 0$ transitions of CCH and CN and the $J = 2_{1,2} \rightarrow 1_{0,1}$ transition of c-C_3H_2, conducted with the new Atacama Large Millimeter/submillimeter Array (ALMA) prototype 12 m antenna of the Arizona Radio Observatory at 3 mm in wavelength. Column densities of the three species were calculated to be N_{tot}(CCH) $\sim$ (0.8–6.6) $\times$ 10^{12} cm^{-2}, N_{tot}(c-C_3H_2) $\sim$ (0.3–5.9) $\times$ 10^{11} cm^{-2}, and N_{tot}(CN) $\sim$ (0.7–7.4) $\times$ 10^{12} cm^{-2}, corresponding to fractional abundances, with respect to H_2, of f(CCH) $\sim$ (1.1–8.8) $\times$ 10^{-7}, f(c-C_3H_2) $\sim$ (0.4–7.9) $\times$ 10^{-8}, and f(CN) $\sim$ (0.9–9.9) $\times$ 10^{-7}. Surprisingly, the abundances are comparable to those measured in younger planetary nebulae (PNe), indicating that predicted photodestruction processes for gas-phase molecules are inefficient in these objects, even over long timescales. The distributions of these two hydrocarbons in the Helix appear to be correlated, with a ratio of [CCH]/[c-C_3H_2] $\sim$ 5–80 and an average value of 29 $\pm$ 6—remarkably similar to both the range ([CCH]/[c-C_3H_2] $\sim$ 11–53) and average value (28.2 $\pm$ 1.4) found in diffuse clouds. The abundances of CCH, c-C_3H_2, and CN in the Helix are also factors of 10–100 greater than those measured in diffuse gas. These results suggest that molecular ejecta from PNe are a possible external source for polyatomic species found in diffuse clouds, including C_{60}.

Key words: astrochemistry – ISM: molecules – planetary nebulae: individual (NGC 7293) – radio lines: ISM

1. Introduction

The presence of polyatomic molecules in diffuse clouds remains unexplained. Given their low densities of 10–100 cm^{-3}, models have predicted that such clouds could only foster and sustain diatomic species (e.g., van Dishoeck & Black 1986). Recently, however, a variety of polyatomic molecules has been detected in these objects, including HCN, HNC, CCH, HCO^+, H_2S, and c-C_3H_2 (e.g., Liszt et al. 2006; Gerin et al. 2011). Even more remarkable, there is strong evidence for the presence of both C_{60} and C_{60}^+ in these low-density sources, as carriers of a few of the diffuse interstellar bands (DIBs; Campbell et al. 2015; Berné et al. 2017). The in situ formation of such complex molecules in diffuse clouds is extremely difficult (Snow & McCall 2006), given their low densities, suggesting an alternative, external source.

One possible origin of the complex molecular material in diffuse clouds are planetary nebulae (PNe). There is a natural connection between these objects, as PNe supply most of the matter to the diffuse interstellar medium (ISM; Dorschner & Henning 1995). Furthermore, some PNe are known to contain C_{60} (e.g., García-Hernández et al. 2012), as well as a substantial number of other polyatomic molecules, including HCN, HNC, CCH, HCO^+, H_2CO, N_2H^+, and SO_2 (e.g., Zhang et al. 2008; Zack & Ziurys 2013; Edwards & Ziurys 2014; Schmidt & Ziurys 2016, 2017a, 2017b). The PN phase follows the asymptotic giant branch (AGB) and is the evolutionary path for most (low- and intermediate-mass) stars. PNe are therefore quite common. Extreme ultraviolet (UV) radiation on the PN track, however, is emitted from the central star as it evolves into a white dwarf—$\sim 10^5$ times that of the general ISM. It is predicted that such radiation in time would destroy all molecular material by the end of the PN phase (e.g., Redman et al. 2003).

Recent observations have shown otherwise. Several older nebulae contain polyatomic molecules with considerable abundances (e.g., Zeigler et al. 2013; Schmidt & Ziurys 2017a). In fact, such abundances appear to remain fairly constant with the age of the nebulae across their life span of $\sim$10,000 years (Schmidt & Ziurys 2016, 2017a, 2017b). The molecular material could be "fossil" species of the former AGB shell and/or be created in the nebulae, possibly by gas-phase reactions or from fragmentation of larger molecules such as C_{60} or even hydrogenated amorphous carbon (HACs; e.g., Duley et al. 2015). The molecules in PNe also appear to be present in dense clumps, mixed with dust, which are self-shielding—consistent with slow dispersion of molecular material from these nebulae into the diffuse ISM (e.g., Zack & Ziurys 2013; Edwards et al. 2014).

The very evolved Helix Nebula (NGC 7293), with an estimated age of $\sim$11,000 years (Meaburn et al. 2008), offers an excellent opportunity to study the fate of molecules in the final stages of PNe. Because of its close proximity to Earth (distance of $\sim$219 pc; Harris et al. 2007), it has a large angular extent of over 1000″. Its unusual geometry has been interpreted as a helix, an equatorial ring with arcs and filaments, and two disks tilted with respect to each other (e.g., O'Dell et al. 2004). Recent mapping in HCO^+ has shown that Helix is actually a bipolar nebula oriented nearly along the line of sight (Zeigler et al. 2013). At one position near the western edge of the nebula, (−372″, 0″) from the central star, various molecules have been detected, including HCN, CN, HNC, HCO^+, CCH,

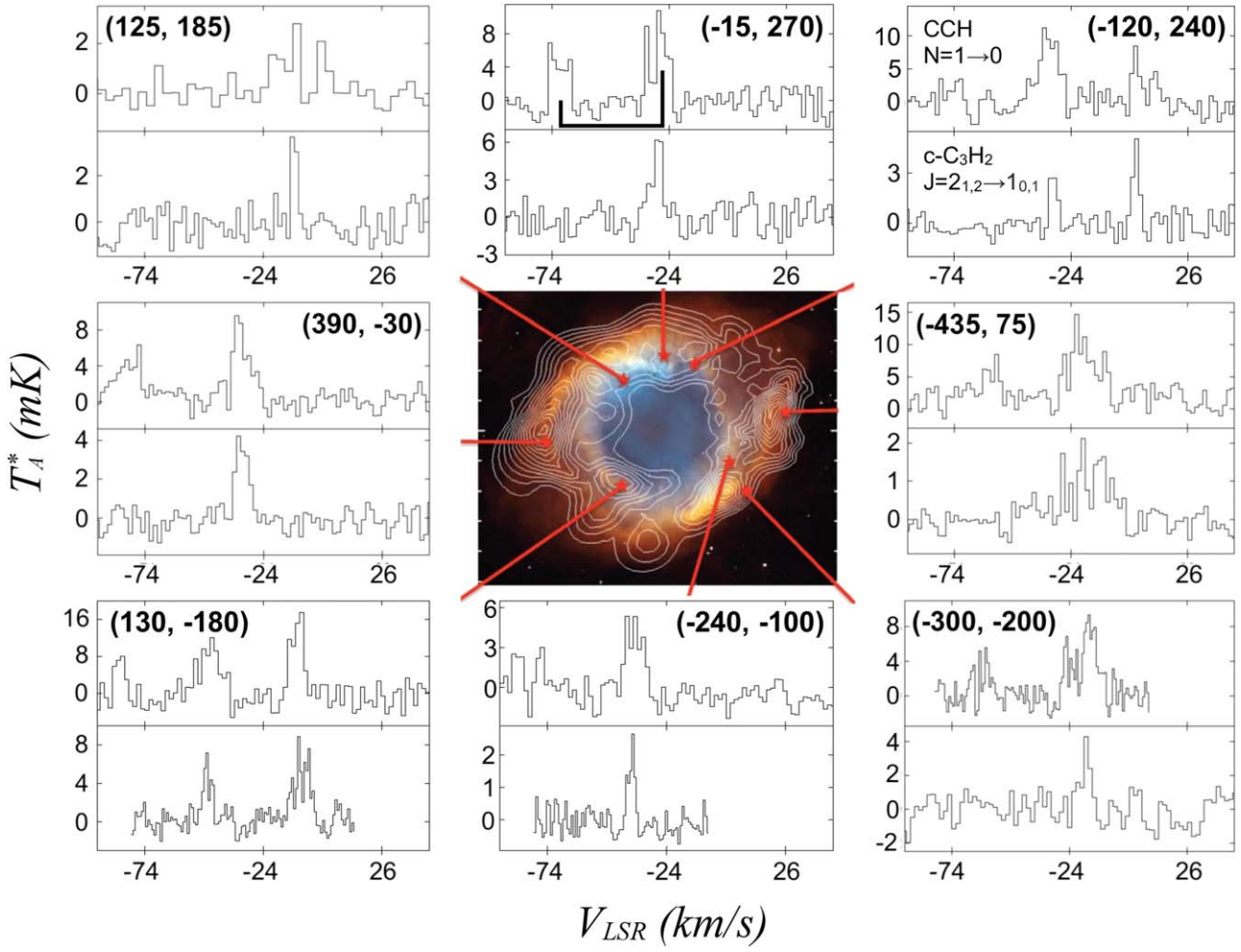

Figure 1. Spectra of the $N = 1 \rightarrow 0$ transition of CCH (upper panel) and the $J_{Ka,Kc} = 2_{1,2} \rightarrow 1_{0,1}$ transition of c-C_3H_2 (lower panel) observed toward eight positions in the Helix Nebula using the ARO 12 m. Positions are indicated in the optical image, which is overlaid with contours tracing HCO^+ emission (see Zeigler et al. 2013). Spectral resolution is 500 kHz, with a few exceptions: 250 kHz resolution was used at the (+130″, −180″) and (−240″, −100″) positions for c-C_3H_2 and at (−300″, −200″) for CCH. For the (+125″, +185″) positions, the resolution for CCH is 1 MHz. The R.A. and decl. offsets for each position are given in arcseconds in the upper left corner of each panel. The CCH hyperfine pattern is indicated on the (−15″, 270″) spectrum. The figure shows that both molecules are widespread in the Helix.

c-C_3H_2, and H_2CO (Bachiller et al. 1997a; Tenenbaum et al. 2009). Further observations by Zack & Ziurys (2013) and Schmidt & Ziurys (2017a) revealed that HCO^+, H_2CO, HCN, and HNC are present at eight other representative positions across the nebula, demonstrating the widespread distribution of polyatomic molecules. Zeigler et al. (2013) additionally showed that HCO^+ emission traces the entire optical, R-band image, as do CO and H_2 (e.g., Young et al. 1999). Furthermore, the molecular abundances of these molecules are comparable to those in much younger nebulae, such as NGC 7027 or NGC 6537 (Zhang et al. 2008; Edwards & Ziurys 2013; Schmidt & Ziurys 2016, 2017a, 2017b). These measurements indicate that significant amounts of molecular material are likely being ejected into the diffuse ISM by the Helix Nebula.

Although polycyclic aromatic hydrocarbons have yet to be detected in the Helix, Young et al. (1997) suggest that the nebula is carbon-rich. Therefore, the presence and distribution of simple hydrocarbons such as CCH and c-C_3H_2 are of interest, as they may tracer larger C-rich species such as fullerenes and HACs. Both CCH and c-C_3H_2 had been previously identified at one position, (−372″, 0″); however, this location may not be representative of the Helix as a whole. More extensive observations are essential to formulate any general conclusions on general hydrocarbon chemistry and larger carbonaceous structures. We have consequently carried out observations of CCH and c-C_3H_2 at the eight additional positions in the Helix previously sampled in H_2CO, HCN, and HNC. We have detected these molecules at all positions, as well as CN, establishing their ubiquity throughout this aging nebula. Outside of the Helix, c-C_3H_2 has been identified in only one other PN: NGC 7027. In this Letter, we present our observations and analysis, and discuss the implications of this work for diffuse cloud chemistry.

2. Observations

Measurements of the $N = 1 \rightarrow 0$ transitions of CN and CCH at 113.491 GHz and 87.317 GHz, respectively, and the $J = 2_{1,2} \rightarrow 1_{0,1}$ transition of c-C_3H_2 at 85.338 GHz were conducted using the 12 m Atacama Large Millimeter/submillimeter Array (ALMA) prototype antenna of the Arizona Radio Observatory (ARO) on Kitt Peak, Arizona between 2014 December and 2018 February. The observations were performed using the dual-polarization, 3 mm receiver employing sideband-separating mixers, with a typical rejection,

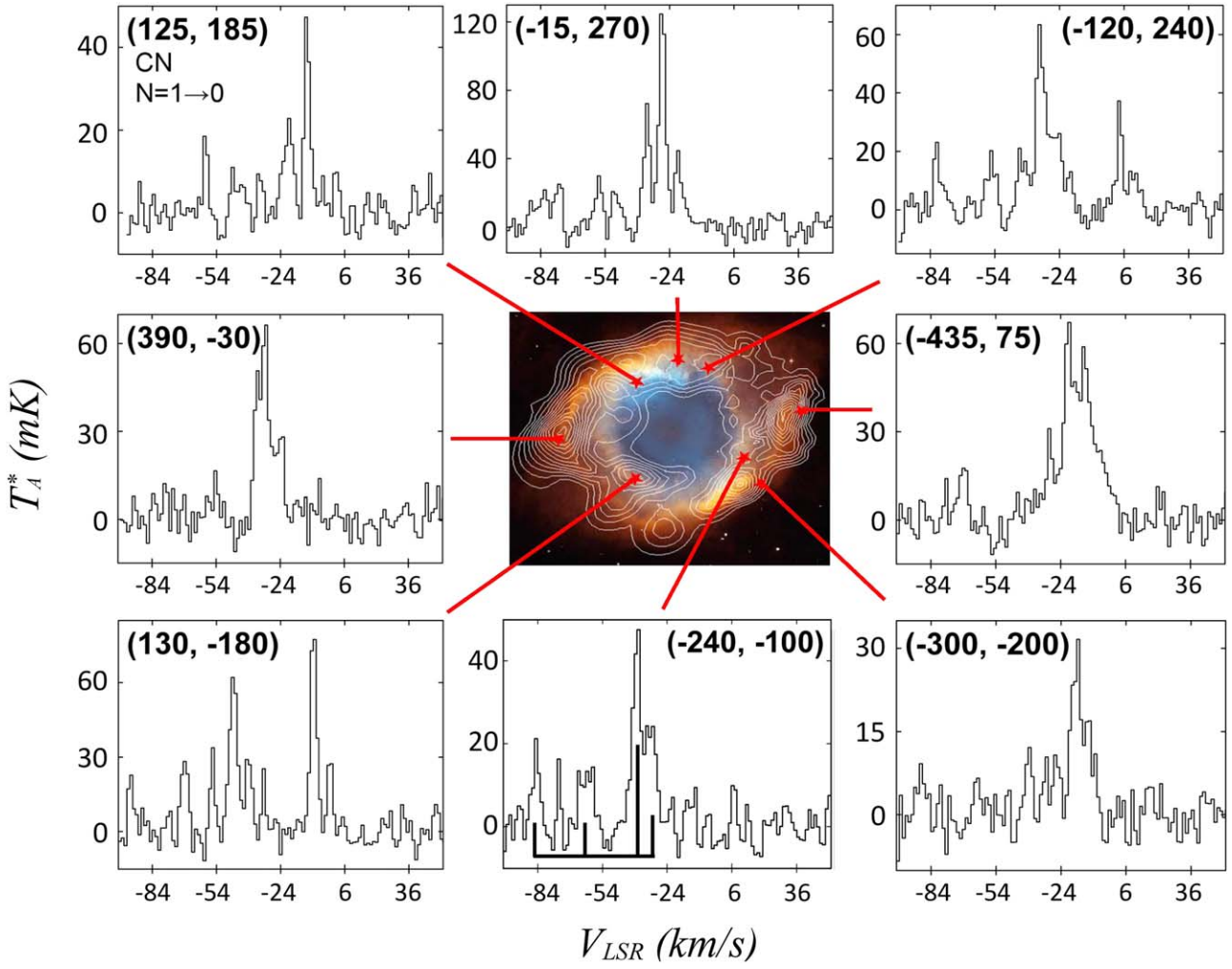

Figure 2. Spectra of the $N = 1 \rightarrow 0$ transition of CN observed toward eight positions in the Helix Nebula as in Figure 1, using the ARO 12 m. Spectral resolution is 500 kHz. The CN hyperfine pattern is shown for the single velocity component on the $(-240'', -100'')$ spectrum. CN is clearly present at all observed positions.

intrinsic to the mixer architecture, of 16 dB. The temperature scale, T_A^*, was determined by the chopper wheel method; the main beam brightness temperature (T_R) is then $T_R = T_A^*/\eta_b$, where η_b is the main beam efficiency. Two of three filter banks with 250 kHz, 500 kHz, and 1 MHz resolutions were employed as backends, depending on the molecule, operated in parallel mode for the two receiver polarizations. The beam size ranged from $\theta_b \sim 55''$–$74''$.

The observed positions are those studied by Zack & Ziurys (2013) and Schmidt & Ziurys (2017a), which represent the nebula as a whole, and are given in arcseconds from the central star (J2000.0 $\alpha = 22^h29^m38\overset{s}{.}6$, $\delta = -20°50'18''$). All observations were conducted in position-switching mode with an azimuth offset of $+30'$. Local oscillator shifts were conducted to test image contamination, and pointing was checked regularly using continuum sources.

3. Results and Analysis

CN, CCH, and c-C_3H_2 were detected at all eight positions in the Helix, as shown in Figures 1 and 2. Figure 1 displays the CCH (upper) and c-C_3H_2 (lower) spectra observed at each position. The hyperfine structure is indicated below the data in black for the $(-15'', 270'')$ position, which has only a single velocity component. Both the $F = 2 \rightarrow 1$ and $F = 1 \rightarrow 0$ hyperfine components of the $N = 1 \rightarrow 0$, $J = 3/2 \rightarrow 1/2$ transition of CCH were observed. Some positions exhibit more than one velocity component, as seen in H_2CO, HCN, and HCO^+ (Zack & Ziurys 2013; Schmidt & Ziurys 2017a).

Figure 2 presents the $N = 1 \rightarrow 0$, $J = 3/2 \rightarrow 1/2$ spectra of CN for each position. The hyperfine structure ($F = 3/2 \rightarrow 1/2$, $F = 5/2 \rightarrow 3/2$, $F = 1/2 \rightarrow 1/2$, $F = 3/2 \rightarrow 3/2$, and $F = 1/2 \rightarrow 3/2$ components) for this radical is displayed under the data for the $(-240'', -100'')$ position, which also has a single velocity feature. The CN line profiles for this source are particularly complex due to its extensive hyperfine structure. CN emission is typically more intense than that of CCH or c-C_3H_2.

Spectral modeling was carried out to deconvolve the velocity structure from the hyperfine components in CCH and CN, assuming the optically thin, LTE limit, as is consistent with the observed line profiles. Relative intensities and frequencies of the hyperfine lines were taken from Ziurys et al. (1982) and Skatrud et al. (1983). Velocity features at each position were well established from our previous works (Zack & Ziurys 2013). Line intensities, LSR velocities, and line widths were adjusted to match the observed features. Examples of the modeled spectra are shown in Figure 3. Here, the observed CN (upper) and CCH (lower) spectra for the $(130'', -180'')$ position are shown in blue (or black), while the fits are overlaid

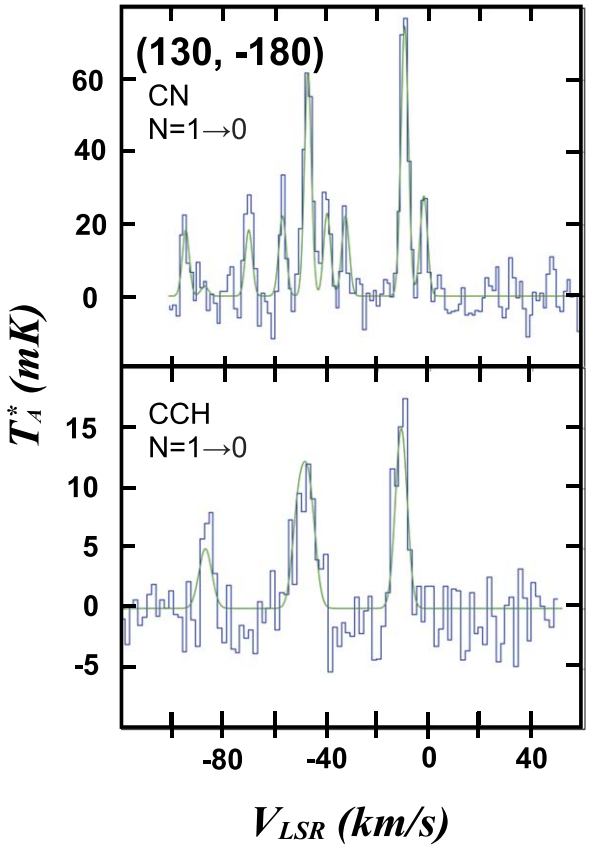

Figure 3. Spectra of CN (upper) and CCH (lower) at the (130″, −180″) position (blue or black), overlaid with the modeling results (green or gray scale). The fitting accounts for the two velocity components (−10 and −47 km s^{-1}) at this position and respective hyperfine structures of the $N = 1 \rightarrow 0$ lines of CN and CCH.

in green (or gray scale). For c-C_3H_2, only the velocity structure had to be considered.

The resultant line parameters T_A^* and $V_{\rm LSR}$ and line widths $\Delta V_{1/2}$ from the analysis for all molecules are summarized in Table 1. Only the strongest hyperfine lines for CCH and CN are presented in the table. Line intensities are ∼0.002–0.120 K. The LSR velocities and line widths are comparable to those measured for CO, HCO^+, and H_2CO by Zack & Ziurys (2013).

CN, CCH, and c-C_3H_2 column densities were estimated using the non-LTE radiative transfer code RADEX (van der Tak et al. 2007). Collisional rates for both CCH and c-C_3H_2 are given in the Leiden Atomic and Molecular Database (LAMDA; Schöier et al. 2005), as well as those for the hyperfine levels in CN with para-H_2. Collisional rates for ortho-H_2 were determined from the fine structure rates of Kalugina et al. (2013) using the infinite-order-sudden (IOS) approximation. Inelastic hyperfine structure rate coefficients $k_{N,J,F\rightarrow N'J'F'}$ for $^2\Sigma$ molecules may be obtained from the $N = 0$, $J = 1/2$ fine structure coefficients $k^{\rm IOS}_{0,\frac{1}{2}\rightarrow L,L+\frac{1}{2}}(T)$ using the following equation (Alexander 1982):

$$k^{\rm IOS}_{NJF\rightarrow N'J'F'}(T) = (2J+1)(2J'+1)(2F'+1)\sum_L \frac{2L+1}{L+1} \times \begin{pmatrix} J' & L & J \\ -1/2 & 0 & 1/2 \end{pmatrix}^2 \begin{Bmatrix} J & J' & L \\ F' & F & I \end{Bmatrix}^2 \times \frac{1}{2}[1-\varepsilon(-1)^{J+J'+L}]k^{\rm IOS}_{0,\frac{1}{2}\rightarrow L,\,L+\frac{1}{2}}(T). \quad (1)$$

The collisional rates were then scaled to account for the IOS approximation, which assumes that rotational level spacing is insignificantly small (Neufeld & Green 1994). Further details can be found in Faure & Lique (2012).

RADEX has three input parameters: column density, H_2 density, and gas kinetic temperature $T_{\rm K}$, which are used to model the main beam brightness temperatures $T_{\rm R}$. As only one rotational transition was observed for each molecule, $T_{\rm K}$ and the H_2 densities for each position and velocity component were set to those found by Zack & Ziurys (2013), based on CO, HCO^+, and H_2CO. These values are $T_{\rm K} \sim 15$–40 K and $n(H_2) \sim (0.1–5) \times 10^5$ cm^{-3}. CN, CCH, and c-C_3H_2 possess dipole moments of 1.45 D (Thomson & Dalby 1968), 0.77 D (Woon 1995), and 3.27 D (Lovas et al. 1992), respectively—a similar range to those of HCO^+, H_2CO, and CO (3.9 D, 2.33 D, and 0.1 D). An H_2 and c-C_3H_2 ortho-para ratio of 3:1 was assumed. The fractional abundances were derived using the average H_2 column density determined by Zack & Ziurys (2013).

Results from this analysis are given in Table 2, which presents column densities $N_{\rm tot}$ and fractional abundances f for CN, CCH, and c-C_3H_2 in the Helix. Values determined fall in the ranges $N_{\rm tot}$(CN) ∼ (0.7–7.4) × 10^{12} cm^{-2}, $N_{\rm tot}$(CCH) ∼ (0.8–6.6) × 10^{12} cm^{-2}, and $N_{\rm tot}$(c-C_3H_2) ∼ (0.3–5.9) × 10^{11} cm^{-2}. Fractional abundances were estimated to be f(CN) ∼ (0.9–9.9) × 10^{-7}, f(CCH) ∼ (1.1–8.8) × 10^{-7}, and f(c-C_3H_2) ∼ (0.4–7.9) × 10^{-8}. These values are similar to those determined for the position (−372″, 0″) by Tenenbaum et al. (2009), who found f(CCH) ∼ 10^{-6} and f(c-C_3H_2) ∼ 3.0 × 10^{-8}.

4. Discussion

4.1. Widespread Distribution of Basic Hydrocarbons in the Helix

CCH, c-C_3H_2, and CN are clearly present at all measured positions across the Helix, as were HCN, HNC, HCO^+, and H_2CO, with a virtually identical velocity structure (Zack & Ziurys 2013; Schmidt & Ziurys 2017a). As observations of HCO^+ by Zeigler et al. (2013) have demonstrated, these positions are representative of the nebula and suggest that these molecules are present throughout the object, except for the central ionized gas traced by He II. Furthermore, the abundances vary by approximately an order of magnitude across the entire nebula, suggesting well-mixed gas. The [CCH]/[c-C_3H_2] ratio falls in the range ∼5–80, with an average value of 29. CCH and c-C_3H_2 are evidently common constituents of this very old PN with similar spatial distributions.

CN is predicted to form from the photodissociation of HCN (e.g., Nejad & Millar 1987). This relationship may be reflected in the [CN]/[HCN] ratio. Across the Helix, this ratio was found to be ∼1–10, analogous to other nebulae (∼2–12; Bachiller et al. 1997a; Zhang et al. 2008; Edwards & Ziurys 2013, 2014), with the exception of two positions: (−240″, −100″) and (−15″, 270″). Here, the −38 and −29 km s^{-1} components exhibited higher values of [CN]/[HCN] ∼ 20–30. In contrast, the [HCN]/[HNC] ratio measured in the Helix at identical positions and velocities was fairly constant at ∼1–4. These results suggest that HCN and HNC share a common precursor, likely $HCNH^+$, while CN may be produced by other avenues not directly involving HCN. The typical value of the [CN]/[HCN] ratio in circumstellar AGB envelopes is ∼0.45 (Bachiller et al. 1997b).

Table 1
Observations of CN, CCH, and c-C_3H_2 toward the Helix Nebula[a]

Offset ($\Delta\alpha$, $\Delta\delta$)	Molecule	Transition	T_A^* (mK)	V_{LSR} (km s^{-1})	$\Delta V_{1/2}$ (km s^{-1})
(130, −180)	CN	$F = 5/2 \rightarrow 3/2$[b]	62 ± 5	−47.3 ± 1.3	3.2 ± 1.3
			75 ± 5	−9.7 ± 1.3	3.4 ± 1.3
	CCH	$F = 2 \rightarrow 1$[c]	10 ± 3	−47.0 ± 1.7	5.9 ± 1.7
			15 ± 3	−11.0 ± 1.7	5.4 ± 1.7
	c-C_3H_2	$J_{Ka,Kc} = 2_{1,2} \rightarrow 1_{0,1}$[d]	7.2 ± 1	−48.0 ± 1.7	2.5 ± 1.7
			8 ± 1	−9.0 ± 1.7	6.0 ± 3.4
(390, −30)	CN	$F = 5/2 \rightarrow 3/2$[b]	66 ± 7	−33.5 ± 1.3	6.0 ± 1.3
	CCH	$F = 2 \rightarrow 1$[c]	9 ± 1	−34.0 ± 1.7	9.0 ± 1.7
	c-C_3H_2	$J_{Ka,Kc} = 2_{1,2} \rightarrow 1_{0,1}$	4 ± 1	−34.3 ± 1.7	6.5 ± 1.7
(−240, −100)	CN	$F = 5/2 \rightarrow 3/2$[b]	48 ± 6	−39.2 ± 1.3	5.7 ± 1.3
	CCH	$F = 2 \rightarrow 1$[c]	5.3 ± 2	−39.0 ± 1.7	7.0 ± 1.7
	c-C_3H_2	$J_{Ka,Kc} = 2_{1,2} \rightarrow 1_{0,1}$[d]	2.7 ± 1	−39.0 ± 0.9	2.5 ± 1.7
(−15, 270)	CN	$F = 5/2 \rightarrow 3/2$[b]	72 ± 15	−35.7 ± 1.3	3.5 ± 1.3
			100 ± 15	−28.7 ± 1.3	3.7 ± 1.3
	CCH	$F = 2 \rightarrow 1$[c]	9 ± 3	−30.5 ± 1.7	7.0 ± 1.7
			∼3	∼−35	∼6.0
	c-C_3H_2	$J_{Ka,Kc} = 2_{1,2} \rightarrow 1_{0,1}$	3 ± 1[e]	−34.6 ± 1.7	3.2 ± 1.7
			6 ± 1[e]	−29.9 ± 0.8	3.2 ± 1.7
(−372, 0)	CN	$F = 5/2 \rightarrow 3/2$[b]	120 ± 15	−15.3 ± 1.3	4.4 ± 1.3
(125, 185)	CN	$F = 5/2 \rightarrow 3/2$[b]	11 ± 6[e]	−24.5 ± 1.3	2.5 ± 1.3
			23 ± 6[e]	−21.3 ± 1.3	3.0 ± 1.3
			41 ± 6	−12.7 ± 1.3	2.9 ± 1.3
	CCH	$F = 2 \rightarrow 1$[c,f]	1.5 ± 0.5[e]	−21.0 ± 1.7	5.9 ± 1.7
			2.8 ± 0.5[e]	−13.0 ± 1.7	4.0 ± 1.7
			2.1 ± 0.5	−1.0 ± 1.7	4.7 ± 1.7
	c-C_3H_2	$J_{Ka,Kc} = 2_{1,2} \rightarrow 1_{0,1}$	3.5 ± 0.5	−12.3 ± 1.7	2.8 ± 1.7
(−435, 75)	CN	$F = 5/2 \rightarrow 3/2$[b]	30 ± 5[e]	−30.3 ± 1.3	2.5 ± 1.3
			60 ± 3[e]	−21.4 ± 1.3	6.2 ± 1.3
			36 ± 4[e]	−13.6 ± 1.3	6.2 ± 3.9
	CCH	$F = 2 \rightarrow 1$[c]	11 ± 3[e]	−21.0 ± 3.4	9.7 ± 1.7
			4 ± 1[e]	−11.5 ± 6.8	9.4 ± 1.7
	c-C_3H_2	$J_{Ka,Kc} = 2_{1,2} \rightarrow 1_{0,1}$	1.5 ± 0.5	−29.0 ± 1.7	3.3 ± 1.7
			1.5 ± 0.5	−21.0 ± 1.7	4.8 ± 1.7
			1.5 ± 0.5	−13.0 ± 1.7	6.0 ± 1.7
(−300, −200)	CN	$F = 5/2 \rightarrow 3/2$[b]	11 ± 2	−27.6 ± 1.3	2.5 ± 1.3
			19 ± 2[e]	−20.3 ± 1.3	2.7 ± 1.3
			31 ± 2[e]	−17.1 ± 1.3	2.9 ± 1.3
	CCH	$F = 2 \rightarrow 1$[c,d]	6 ± 2[e]	−24.5 ± 1.7	4.5 ± 1.7
			8 ± 2[e]	−16.0 ± 1.7	4.7 ± 1.7
	c-C_3H_2	$J_{Ka,Kc} = 2_{1,2} \rightarrow 1_{0,1}$	4 ± 1	−17.8 ± 1.7	3.3 ± 1.7
(−120, 240)	CN	$F = 5/2 \rightarrow 3/2$[b]	64 ± 5	−34.2 ± 1.3	5.6 ± 1.3
			38 ± 5	3.1 ± 1.3	4.0 ± 1.3
	CCH	$F = 2 \rightarrow 1$[c]	10 ± 1	−34.0 ± 1.7	5.0 ± 1.7
			8.4 ± 1	3.0 ± 1.7	3.0 ± 1.7
	c-C_3H_2	$J_{Ka,Kc} = 2_{1,2} \rightarrow 1_{0,1}$	3 ± 1	−32.5 ± 3.4	3.8 ± 1.7
			5 ± 1	2.5 ± 1.7	3.8 ± 1.7

Notes.
[a] Measured with 500 kHz resolution unless noted; only the strongest hyperfine components are listed.
[b] Blend of $F = 5/2 \rightarrow 3/2$ and $3/2 \rightarrow 1/2$ hyperfine components (see the text).
[c] $F = 1 \rightarrow 0$ hyperfine component also measured (see the text).
[d] Measured with 250 kHz resolution.
[e] Partially blended velocity components.
[f] Measured with 1 MHz resolution.

Abundances for CN, CCH, and c-C_3H_2 have also been measured in a few other PNe. Those for CN are in the range ∼(0.7–6.1) × 10^{-7}, which includes younger (NGC 7027 and NGC 6537) and older (M2-48, M4-9 and NGC 6781) objects (Bachiller et al. 1997a; Zhang et al. 2008; Edwards & Ziurys 2013, 2014). These values are comparable to those found for the Helix ((0.9–9.9) × 10^{-7}). CCH has been identified in 11 other PNe spanning ages ∼700–11,000 years, with abundances of ∼(0.2–47) × 10^{-7} (Zhang et al. 2008; Edwards & Ziurys 2013; Schmidt & Ziurys 2017b)—again similar to those measured for the Helix ((1.1–8.8) × 10^{-7}). Remarkably, c-C_3H_2 has previously been detected in only one other PN, NGC 7027, with $f \sim 8.3 \times 10^{-9}$ (Zhang et al. 2008) —comparable to the Helix values of $f \sim$ (0.4–7.9) × 10^{-8}.

Table 2
Column Densities and Abundances for CCH, c-C_3H_2, and CN in the Helix Nebula

Position	V_{LSR}	N_{tot}(CN) (10^{12} cm^{-2})	N_{tot}(CCH) (10^{12} cm^{-2})	N_{tot}(c-C_3H_2) (10^{11} cm^{-2})	f (CN) (10^{-7})	f(CCH) (10^{-7})	f(c-C_3H_2) (10^{-8})	CN/HCN	CCH/c-C_3H_2
(130, −180)	−47	2.9 ± 0.4	3.6 ± 0.3	1.1 ± 0.4	3.9 ± 0.5	4.8 ± 0.4	1.5 ± 0.5	8.0 ± 1.8	32.0 ± 11.0
	−10	3.7 ± 0.5	4.9 ± 0.1	2.8 ± 0.6	4.9 ± 0.7	6.5 ± 0.1	3.7 ± 0.8	9.6 ± 3.0	17.6 ± 3.8
(390, −30)	−33	5.4 ± 0.5	4.4 ± 0.3	2.0 ± 0.3	7.2 ± 0.7	5.9 ± 0.4	2.7 ± 0.4	6.0 ± 0.8	21.9 ± 3.6
(−240, −100)	−38	4.1 ± 0.1	2.3 ± 0.3	0.4 ± 0.1	5.5 ± 0.1	3.1 ± 0.4	0.5 ± 0.1	22.9 ± 3.8	62.0 ± 14.8
(−15, 270)	−35	3.3 ± 0.4	1.0 ± 0.2	0.6 ± 0.2	4.4 ± 0.5	1.3 ± 0.3	0.9 ± 0.3	7.5 ± 2.1	14.4 ± 5.8
	−29	6.5 ± 1.3	4.9 ± 0.9	1.3 ± 0.1	8.7 ± 1.7	6.5 ± 1.2	1.7 ± 0.1	34.8 ± 14.3	38.2 ± 7.4
(−120, 240)	−33	4.6 ± 0.4	2.7 ± 0.3	0.7 ± 0.1	6.1 ± 0.5	3.6 ± 0.4	0.9 ± 0.1	7.3 ± 1.6	40.0 ± 6.3
	4	2.0 ± 0.2	1.4 ± 0.3	1.3 ± 0.2	2.7 ± 0.3	1.9 ± 0.4	1.7 ± 0.3	7.7 ± 2.0	11.2 ± 3.0
(125, 185)	−25	1.1 ± 0.3	⋯	⋯	1.5 ± 0.4	⋯	⋯	0.9 ± 0.3	⋯
	−20	2.7 ± 0.5	1.6 ± 0.2	⋯	3.6 ± 0.7	2.1 ± 0.3	⋯	1.2 ± 0.4	⋯
	−13	2.1 ± 0.6	0.8 ± 0.2	1.6 ± 0.8	2.8 ± 0.8	1.1 ± 0.3	2.1 ± 1.1	1.8 ± 0.5	5.2 ± 3.1
	−1	⋯	0.9 ± 0.1	⋯	⋯	1.2 ± 0.1	⋯	⋯	⋯
(−435, 75)	−29	1.0 ± 0.2	⋯	0.3 ± 0.1	1.3 ± 0.3	⋯	0.4 ± 0.1	6.2 ± 1.7	⋯
	−21	5.5 ± 0.7	6.6 ± 0.1	0.8 ± 0.1	7.3 ± 0.9	8.8 ± 0.1	1.1 ± 0.1	3.0 ± 0.5	80.0 ± 7.3
	−13	4.5 ± 2.0	3.3 ± 0.5	2.0 ± 0.5	6.0 ± 2.7	4.4 ± 0.7	2.7 ± 0.7	2.8 ± 1.3	16.3 ± 5.0
(−300, −200)	−27	0.7 ± 0.3	4.0 ± 0.7	⋯	0.9 ± 0.4	5.3 ± 0.9	⋯	1.6 ± 0.8	⋯
	−21	1.3 ± 0.5	⋯	⋯	1.7 ± 0.7	⋯	⋯	2.2 ± 1.0	⋯
	−17	2.2 ± 0.9	5.6 ± 1.2	5.9 ± 1.8	2.9 ± 1.2	7.5 ± 1.6	7.9 ± 2.4	0.9 ± 0.4	9.5 ± 3.5
(−372, 0)	−15	7.4 ± 0.3	⋯	⋯	9.9 ± 0.4	⋯	4.0	⋯	⋯

These results indicate that the abundances of CN, CCH, and c-C_3H_2 measured in older PNe like the Helix are not markedly different from those of younger PNe, and remain relatively constant with nebular age.

4.2. Molecular Synthesis of CCH and c-C_3H_2 in the Helix

It is unclear whether the observed molecules in PNe are remnant AGB material, or have been resynthesized in the PN phase. As discussed by Schmidt & Ziurys (2017b), the CCH abundance decreases by a factor of 5, on average, from the AGB to the PN stages. For c-C_3H_2, fewer sources have been studied, but AGB abundances for this species appear to fall in the range $\sim 10^{-8}$–10^{-7} (Woods et al. 2003). This molecule therefore undergoes an abundance decrease of a factor of ∼10 in PNe. This evolution is not inconsistent with molecular survival following AGB production. These molecules might then be involved in the synthesis of fullerenes, in the "bottom-up" scenario, which utilizes C_2 as a building block (Dunk et al. 2012; Schmidt & Ziurys 2017b).

On the other hand, both CCH and c-C_3H_2, as hydrocarbons, could also be replenished in situ in the nebulae from UV degradation of larger carbon-bearing structures, including fullerenes and possibly HACs. C_{60} and C_{70} have been identified in a few PNe, and certain infrared features, such as those near 6–9, 9–13, 15–20, and 25–35 μm, have been attributed to HACs (e.g., García-Hernández et al. 2012). This "top-down" synthesis is thought to produce C_2 units in the destruction process (e.g., Micelotta et al. 2012; Berné et al. 2015). The ubiquitous presence of CCH, the millimeter-wave proxy for C_2, which does not have a pure rotational spectrum, may indicate such chemical breakdown. Furthermore, Duley et al. (2015) argue that the photon-induced decomposition of HACs could explain the presence of c-C_3H_2 in the ISM, based on laboratory experiments (see also Alata et al. 2014).

Another synthetic route to CCH and c-C_3H_2 in PNe is through gas-phase photochemistry, possibly linked to acetylene. The dissociative recombination of $C_3H_3^+$ is thought to lead to c-C_3H_2 (Nejad & Millar 1987). This ion is the product of the radiative association of $C_3H^+ + H_2$. Another pathway to c-C_3H_2 is the reaction of C^+ with acetylene and related hydrocarbons (Fuente et al. 2003). CCH may be synthesized by the photodissociation of acetylene in PNe, as speculated by Schmidt & Ziurys (2017b)—the main formation pathway in AGB envelopes.

4.3. Populating Diffuse Clouds

CN, CCH, and c-C_3H_2 are all common constituents of diffuse clouds (e.g., Liszt et al. 2006). The abundance of CN in these objects varies between $f \sim (1.0\text{–}3.5) \times 10^{-8}$, with an average value of 2×10^{-8} and a mean [CN]/[HCN] ratio of ∼6.8 (Liszt & Lucas 2001). For CCH in diffuse clouds, $f \sim (1.6\text{–}4.2) \times 10^{-8}$, corresponding to an average value of $\sim 2.9 \times 10^{-8}$, while abundances for c-C_3H_2 fall in the range $f \sim (0.7\text{–}2.1) \times 10^{-9}$ (Lucas & Liszt 2000). The average abundance for the latter species is $\sim 1.4 \times 10^{-9}$. Additionally, Lucas & Liszt (2000) found a fairly constant abundance ratio for the two hydrocarbons of $[C_2H]/[c\text{-}C_3H_2] \approx 28$. These authors noted that models of quiescent gas-phase chemistry cannot account for the observed amounts of all three molecules by at least an order of magnitude.

More recent observations of CCH and c-C_3H_2 were also conducted toward diffuse (and translucent) clouds by Gerin et al. (2011). These authors detected both molecules in absorption toward star-forming regions and found their abundances to be tightly correlated with $[C_2H]/[c\text{-}C_3H_2] \sim 11$–53, for an average value of 28.2 ± 1.4. They also modeled the chemical formation of both species with a PDR scheme, finding that the measured CCH column densities could be reproduced. In the case of c-C_3H_2, however, calculated values were consistently lower than observed. These authors concluded that in situ formation of this molecule in diffuse gas is unlikely.

The abundances measured in the Helix are consistently 1–2 orders of magnitude higher than those observed in diffuse clouds (f(CN) $\sim (0.9\text{–}9.9) \times 10^{-7}$, f(CCH) $\sim (1.1\text{–}8.8) \times 10^{-7}$, and

$f(\text{c-}C_3H_2) \sim (0.4\text{–}7.9) \times 10^{-8}$). Furthermore, the average [CN]/[HCN] ratio in this nebula is almost identical to that found in diffuse gas (7.3 versus 6.3). Moreover, CCH and c-C_3H_2 have very similar spatial distributions in the Helix, with an average ratio $[C_2H]/[\text{c-}C_3H_2] \sim 29$. Again, these results mimic those found in diffuse clouds. Given these striking similarities, the origin of CN, CCH, the c-C_3H_2 in the diffuse ISM could very well be planetary nebula ejecta. It is noteworthy that the abundance of C_{60} in measured in PNe and PPNe is about a factor of 10–100 greater than found in the diffuse ISM (Berné et al. 2017), also suggesting an origin in PN ejecta.

This research was supported by NSF grant AST-1515568.

References

Alata, I., Cruz-Diaz, G. A., Muñoz Caro, G. M., & Dartois, E. 2014, A&A, 569, A119
Alexander, M. 1982, JChPh, 76, 3637
Bachiller, R., Forveille, T., Huggins, P. J., & Cox, P. 1997a, A&A, 324, 1123
Bachiller, R., Fuente, A., Bujarrabal, V., et al. 1997b, A&A, 319, 235
Berné, O., Cox, N. L. J., Mulas, G., & Joblin, C. 2017, A&A, 605, L1
Berné, O., Montillaud, J., & Joblin, C. 2015, A&A, 577, A133
Campbell, E. K., Holz, M., Gerlich, D., & Maier, J. P. 2015, Natur, 523, 322
Dorschner, J., & Henning, T. 1995, A&ARv, 6, 271
Duley, W. W., Zaidi, A., Wesolowski, M. J., & Kuzmin, S. 2015, MNRAS, 447, 1242
Dunk, P. W., Kaiser, N. K., Hendrickson, C. L., et al. 2012, NatCo, 3, 855
Edwards, J. L., Cox, E. G., & Ziurys, L. M. 2014, ApJ, 791, 79
Edwards, J. L., & Ziurys, L. M. 2013, ApJL, 770, L5
Edwards, J. L., & Ziurys, L. M. 2014, ApJL, 794, L27
Faure, A., & Lique, F. 2012, MNRAS, 425, 740
Fuente, A., Rodríguez-Franco, A., García-Burillo, S., Martín-Pintado, J., & Black, J. H. 2003, A&A, 406, 899
García-Hernández, D. A., Villaver, E., García-Lario, P., et al. 2012, ApJ, 760, 107
Gerin, M., Kaźmierczak, M., Jastrzebska, M., et al. 2011, A&A, 525, A116
Harris, H. C., Dahn, C. C., Canzian, B., et al. 2007, AJ, 133, 631
Kalugina, Y., Kłos, J., & Lique, F. 2013, JChPh, 139, 074301
Liszt, H., & Lucas, R. 2001, A&A, 370, 576
Liszt, H. S., Lucas, R., & Pety, J. 2006, A&A, 448, 253
Lovas, F. J., Suenram, R. D., Ogata, T., & Yamamoto, S. 1992, ApJ, 399, 325
Lucas, R., & Liszt, H. S. 2000, A&A, 358, 1069
Meaburn, J., Lopez, J. A., & Richer, M. G. 2008, MNRAS, 384, 497
Micelotta, E. R., Jones, A. P., Cami, J., et al. 2012, ApJ, 761, 35
Nejad, L. A. M., & Millar, T. J. 1987, A&A, 183, 279
Neufeld, D. A., & Green, S. 1994, ApJ, 432, 158
O'Dell, C. R., McCullough, P. R., & Meixner, M. 2004, AJ, 128, 2339
Redman, M. P., Viti, S., Cau, P., & Williams, D. A. 2003, MNRAS, 345, 1291
Schmidt, D. R., & Ziurys, L. M. 2016, ApJ, 817, 175
Schmidt, D. R., & Ziurys, L. M. 2017a, ApJ, 835, 79
Schmidt, D. R., & Ziurys, L. M. 2017b, ApJ, 850, 123
Schöier, F. L., van der Tak, F. F. S., van Dishoeck, E. F., & Black, J. H. 2005, A&A, 432, 369
Skatrud, D. D., De Lucia, F. C., Blake, G. A., & Sastry, K. V. L. N. 1983, JMoSp, 99, 35
Snow, T. P., & McCall, B. J. , 2006, ARA&A, 44, 367
Tenenbaum, E. D., Milam, S. N., Woolf, N. J., & Ziurys, L. M. 2009, ApJL, 704, L108
Thomson, R., & Dalby, F. W. 1968, CaJPh, 46, 2815
van der Tak, F. F. S., Black, J. H., Schöier, F. L., Jansen, D. J., & van Dishoeck, E. F. 2007, A&A, 468, 627
van Dishoeck, E. F., & Black, J. H. 1986, ApJS, 62, 109
Woods, P. M., Schöier, F. L., Nyman, L. Å, & Olofsson, H. 2003, A&A, 402, 617
Woon, D. E. 1995, CPL, 244, 45
Young, K., Cox, P., Huggins, P. J., Forveille, T., & Bachiller, R. 1997, ApJL, 482, L101
Young, K., Cox, P., Huggins, P. J., Forveille, T., & Bachiller, R. 1999, ApJ, 522, 387
Zack, L. N., & Ziurys, L. M. 2013, ApJ, 765, 112
Zeigler, N., Zack, L. N., Woolf, N. J., & Ziurys, L. M. 2013, ApJ, 778, 16
Zhang, Y., Kwok, S., & Dinh-V-Trung 2008, ApJ, 678, 328
Ziurys, L. M., Saykally, R. J., Plambeck, R. L., & Erickson, N. R. 1982, ApJ, 254, 94